Article

Streamflow Changes in the Headwater Area of Yellow River, NE Qinghai-Tibet Plateau during 1955–2040 and Their Implications

Qiang Ma [1,2], Changlei Dai [1], Huijun Jin [2,3,*], Sihai Liang [4], Victor F. Bense [2,5], Yongchao Lan [2], Sergey S. Marchenko [6] and Chuang Wang [1]

1   Institute of Groundwater in Cold Regions, and School of Hydraulic and Electric Power, Heilongjiang University, Harbin 150040, China; maqiang8002@lzb.ac.cn (Q.M.); daichanglei@126.com (C.D.); wangchuang1202@163.com (C.W.)
2   State Key Laboratory of Frozen Soils Engineering, Northwest Institute of Eco-Environment and Resources, Chinese Academy of Sciences, Lanzhou 730000, China; victor.bense@wul.nl (V.F.B.); lyc@lzb.ac.cn (Y.L.)
3   Northeast-China Observatory and Research-Station of Permafrost Geo-Environment-Ministry of Education, Institute of Cold-Regions Science and Engineering, and School of Civil Engineering, Northeast Forestry University, Harbin 150040, China
4   School of Water Resources and Environment, China University of Geosciences, Beijing 100083, China; liangsh@cugb.edu.cn
5   Hydrology and Quantitative Water Management Group, Department of Environmental Sciences, Wageningen University, 6708PB Wageningen, The Netherlands
6   Permafrost Lab., Geophysical Institute, University of Alaska Fairbanks, Fairbanks, AK 99775, USA; ssmarchenko@alaska.edu
*   Correspondence: hjjin@nefu.edu.cn; Tel.: +86-188-9318-5876

Abstract: Human activities have substantially altered present-day flow regimes. The Headwater Area of the Yellow River (HAYR, above Huanghe'yan Hydrological Station, with a catchment area of 21,000 km^2 and an areal extent of alpine permafrost at ~86%) on the northeastern Qinghai-Tibet Plateau, Southwest China has been undergoing extensive changes in streamflow regimes and groundwater dynamics, permafrost degradation, and ecological deterioration under a warming climate. In general, hydrological gauges provide reliable flow records over many decades and these data are extremely valuable for assessment of changing rates and trends of streamflow. In 1998–2003, the damming of the Yellow River by the First Hydropower Station of the HAYR complicated the examination of the relations between hydroclimatic variables and streamflow dynamics. In this study, the monthly streamflow rate of the Yellow River at Huanghe'yan is reconstructed for the period of 1955–2019 using the double mass curve method, and then the streamflow at Huagnhe'yan is forecasted for the next 20 years (2020–2040) using the Elman neural network time-series method. The dam construction (1998–2000) has caused a reduction of annual streamflow by 53.5–68.4%, and a more substantial reduction of 71.8–94.4% in the drier years (2003–2005), in the HAYR. The recent removal of the First Hydropower Station of the HAYR dam (September 2018) has boosted annual streamflow by 123–210% (2018–2019). Post-correction trends of annual maximum (Q_{Max}) and minimum (Q_{Min}) streamflow rates and the ratio of the Q_{Max}/Q_{Min} of the Yellow River in the HAYR (0.18 and 0.03 m$^3 \cdot$s$^{-1} \cdot$yr^{-1} and −0.04 yr^{-1}, respectively), in comparison with those of precorrection values (−0.11 and −0.004 m$^3 \cdot$s$^{-1} \cdot$yr^{-1} and 0.001 yr^{-1}, respectively), have more truthfully revealed a relatively large hydrological impact of degrading permafrost. Based on the Elman neural network model predictions, over the next 20 years, the increasing trend of flow in the HAYR would generally accelerate at a rate of 0.42 m$^3 \cdot$s$^{-1} \cdot$yr^{-1}. Rising rates of spring (0.57 m$^3 \cdot$s$^{-1} \cdot$yr^{-1}) and autumn (0.18 m$^3 \cdot$s$^{-1} \cdot$yr^{-1}) discharge would see the benefits from an earlier snow-melt season and delayed arrival of winter conditions. This suggests a longer growing season, which indicates ameliorating phonology, soil nutrient availability, and hydrothermal environments for vegetation in the HAYR. These trends for hydrological and ecological changes in the HAYR may potentially improve ecological safety and water supplies security in the HAYR and downstream Yellow River basins.

1. Introduction

Anthropogenic activities (e.g., river damming) can substantially change streamflow regimes. Ye et al. (2003) and Adam et al. (2007) addressed the shifts in seasonal variability of streamflow closely related to dams in large Asian arctic rivers [1,2]. Steufer et al. (2011) noted that the annual average streamflow of large Siberian rivers and the relationship between precipitation and streamflow had been changed by damming issues [3]. Chai et al. (2019) highlighted that, under the damming effects, the streamflow had a negative anomaly in flood seasons and a positive anomaly in drought seasons in comparison with those of the pre-dam period in the Yangtze River [4]. As such, damming can alter streamflow regimes at both inter- and intra-annual scales.

Important shifts in streamflow regimes have been extensively reported in Arctic, boreal, alpine, and high-plateau regions caused by permafrost degradation under a warming climate (e.g., [5–17]). Permafrost degradation will improve hydraulic connectivity between surface and subsurface waters, and among the supra-, intra- and sub-permafrost waters in particular [5,9,10]. A boosted baseflow (e.g., [6,7,11–13]) and a decreased peak flow indicate a shifted intra-annual regime of streamflow, such as flattened hydrographs and decreased ratio of annual maximum/minimum streamflow (Q_{Max}/Q_{Min}) (e.g., [8,14–17]). An increased baseflow and melting ground-ice would boost groundwater recharge and increase groundwater storage upon permafrost thaw (e.g., [10,18–23]). With a catchment area of 21,000 km^2, the Headwater Area of the Yellow River (HAYR, above the Huanghe'yan Hydrological Station) on the northeastern Qinghai-Tibet Plateau (QTP), with widespread discontinuous (~86%) permafrost [24–26], and under a persistently warming and slightly wetting climate, flow regimes of the Yellow River in the HAYR have shown no evident increasing trend in general as reported. Instead, the Yellow River flow showed a general trend of decline during 1955–2019, but the ratio of the Q_{Max}/Q_{Min} demonstrated a slightly increasing trend under permafrost degradation, in contrast to the observed streamflow shifts in other northern and alpine permafrost regions (e.g., [6,7,13,19]).

The HAYR plays key roles in supplying water to the Yellow River and in preserving endemic alpine flora species and relatively pristine alpine ecosystems [27,28]. In the 1990s and 2000s, eco-environmental deterioration in the HAYR has drawn intense and extensive attention of the public, governments, and academic communities. Hydrological and ecological regimes in the HAYR are important to the ecological safety and water supply security of local communities and downstream Yellow River basins [29]. Changes in streamflow are strongly associated with those in vegetation [30–34]. In high Canadian Arctic regions, an 80% increase of vegetation productivity on the Banks Islands is documented and magnitude of greening is closely related to flow accumulation and increasing soil moisture of the catchment [33]. After analyzing long-term discharge and normalized difference vegetation index (NDVI) data, Xu et al. (2013) found strong seasonal consistency between river discharge and NDVI in the Mackenzie River Basin, NWT, Canada [34]. An increasing trend in spring streamflow was observed in Western Arctic Russia, potentially indicating an earlier snowmelt season [35]. By employing phenological parameters from NDVI time series, Zeng et al. (2013) confirmed an earlier start, a later ending, and thus an elongation of the growing season in the Russian Arctic [36]. Therefore, changes in streamflow conditions can be an indicator for changes in vegetation to some extent.

Thus, systematic analyses and interpretations of the real-time streamflow regimes in the HAYR are essential for examining the impact of permafrost degradation on streamflow regimes and ecological implications of streamflow changes. Changes of streamflow in the HAYR in the future would also play important roles in ecological safety and freshwater budgets in local communities and downstream Yellow River Basin [37]. In this paper, the

historical streamflow record in the HAYR was reconstructed by employing the double mass curve method and streamflow data in neighboring downstream hydrological stations (Jimai, Maqu, and Tanag) to obtain the real-time streamflow. Based on the reconstructed streamflow data in the HAYR, the streamflow for the future 20 years was predicted using the artificial neural networks time-series method. The reconstructed streamflow dataset can serve as a fundamental dataset for permafrost hydrology, eco-hydrology and other related studies in the HAYR. Better predictions of streamflow patterns under shifting climate and environment can provide timely scientific support for ecological protection and management and logical planning and utilization of land–water resources.

2. Materials and Methods

2.1. Study Area

The HAYR is a catchment of the Yellow River Basin above the Huanghe'yan (Yellow Riverside) Hydrological Station (33.9°–35.5° N, 95.8°–98.4° E; 4207–5245 m a. s. l.), with a catchment area of about 21,000 km^2 (Figure 1). The HAYR consists of many high elevation intermontane basins and the Yellow River valleys. To the north, the HAYR is bordered by the Buqing and Bur Hanbuda mountains; to the west and south, by the Geshigeya and Baryan Har mountains, respectively [5]. In the intermontane river or lake basins, the landscape is basically flat, or gently sloping; stream channels are largely braided on slopes and meandering in lowlands or valley wetlands.
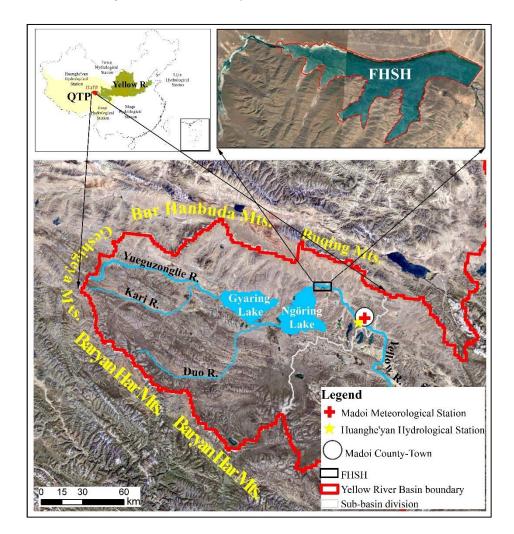

Figure 1. Study sites, stations, and catchment of the Headwater Area of the Yellow River (HAYR) on the northeastern Qinghai-Tibet Plateau in Southwest China (the base map was extracted from Google earth https://us9060.scholar.eu.org/extdomains/earth.google.com/ accessed on 1 September 2020).

The streamflow at Huanghe'yan accounted for 2.75% of the multi-year average of annual streamflow (at the Lijin Hydrological Station in Shandong Province, East China) of the Yellow River to the Pacific Ocean (2008–2017) [38]. In January 1998, the First Hydropower Station of the HAYR (FHSH, height, 18 m; inundated area, ~16.5 km^2), also called the Ngöring Lake Reservoir (Figure 1), started to be built 30 km upstream of the Huanghe'yan Hydrological Station for supplying electricity for the Madoi County-town (Machali town), Qinghai Province. At the beginning, the stream channel was fully blocked with sandbags upstream the working section (dam-site), inducing a sharply decreased streamflow at Huanghe'yan. By January 2007, the FHSH had experienced the stages of building (January 1998 to February 2000), impounding (March 2000 to December 2002), and partial operation (January 2003 to June 2005) due to the persistent low-flow periods in the HAYR. During the period of partial operation, the streamflow in the HAYR was mostly preserved in the reservoir. In 2007, precipitation increased markedly in the HAYR, resulting in a rising streamflow at Huanghe'yan. The incoming water to the FHSH was largely discharged by outflowing from the reservoir due to its limited storage capacity. In October 2016, the FHSH was abandoned. The State Grid started to supply electricity for Madoi. Subsequently, the water-gate of the FHSH was left partly open and the incoming water was largely reserved in the FHSH. In September 2018, the removal of the FHSH was implemented for ecological restoration. Until August 2019, when streamflow data were most updated in this paper, the FHSH was kept open, but not completely removed. Thus, the damming of the FHSH has substantially altered regimes of the streamflow in the HAYR as measured at Huanghe'yan.

The HAYR is dominated by a semiarid alpine climate under the control of alternating monsoons and westerlies. Based on data series at the Madoi Meteorological Station (34.92° N, 98.26° E; 4272.3 m asl) from 1961–2017, the mean annual air temperature (MAAT) ranged from −4.4 to −0.7 °C, with a multi-year average of MAAT at −1.7 °C; annual precipitation was 484-755 mm (corrected for dynamic and other losses), with a multi-year average at 623.0 mm [8].

In the HAYR, discontinuous, sporadic, and isolated permafrost presents and account for ~86% of the catchment area above Huanghe'yan Hydrological Station near Madoi [24–26]. Mean annual ground temperatures, measured at the depth of zero annual amplitude, generally 10–25 m, are higher than −2.0 °C; permafrost in the HAYR is generally thinner than 50–100 m according to borehole measurements [39]. The average active layer thickness (ALT) over the HAYR varied from 1.8 to 2.4 m during the period of 1980–2006 [40]. Ice-rich permafrost is widely distributed in lacustrine marshlands and alluvial-lacustrine plains, and the table of permafrost, sometimes residual, is concentrated at depths of 3.0–10.0 m in the HAYR [5,9,25]. In recent decades, the HAYR has witnessed a marked climate warming of 0.045 °C·yr^{-1} (1961–2017) and subsequent permafrost degradation [5,41,42]. The ALT increased at an average rate of 1.2 cm·yr^{-1} during the period of 1972–2012, and by 2100, the ALT is projected to increase by 2.78–4.39 m and the areal extent of permafrost in the HAYR is forecasted to decrease by 7.5–8.6% under varied carbon emission scenarios [26]. Presence of permafrost can strongly influence the streamflow regimes in permafrost catchments. Schematic in-stream flow generation mechanisms in permafrost catchments are described in Figure 2.
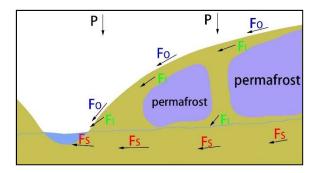
Figure 2. Schematic in-stream flow generation mechanisms in permafrost catchments (P: precipitation; F_O: overflow; F_I: interflow; F_S: saturated flow).

The HAYR is covered by alpine grassland ecosystems, accounting for an areal extent of 93.6% on land surface (Figure 3). In the HAYR, alpine steppes and meadows are widespread and soil types are dominated by Cryic Calcic Aridisols (alpine steppe soils) and Mattic Cryic Cambisols (alpine meadow soils) [39]. Plant species in alpine steppes is dominated by *Stipa purpurea*, *Agropyron cristatum*, *Saussurea arenaria*, and others, and those in alpine meadow, by *Kobresia capillifolia*, *K. humilis*, *Poa alpine*, *S. pseudomalitiosa*, and others [28,43,44]. Brierley et al. (2016) highlighted a significant deterioration of alpine grasslands in the HAYR in the 1980s and 1990s, probably due to diminishing near-surface soil moisture [45] (Figure 3).
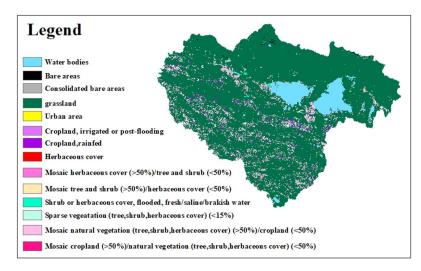

Figure 3. Land-cover types in the Head Water of the Yellow River, northeastern QTP, southwest China (extracted from [46]).

2.2. Data Acquisition

Monthly streamflow data were collected from the Yellow River Conservancy Commission for the Huanghe'yan Hydrological Station and neighboring downstream hydrological stations (Jimai, Maqu and Tanag) from January 1955 to August 2019. During the period of August 1968 to December 1975, the observations of Huanghe'yan Hydrological Station were interrupted and moved 550 m downstream and were rebuilt at the current location; the hydrometeorological data were thus absent during 1968–1975. Streamflow rate at the Huanghe'yan Hydrological Station accounts for 25%, 8% and 4% of that at Jimai, Maqu and Tanag, respectively. Variability of streamflow at Maqu and Tanag hydrological stations has been minimally disturbed by the FHSH. Several other dams (Pandoh, Gaqu, Modoi and Dangcun) built near the Tanag Hydrological Station may have substantially altered the streamflow at Tanag [8]. Thus, the missing observation during these periods was interpolated using monthly streamflow data of Maqu, c.a. 600 km downstream, from January 1976 to December 1997 prior to the building of the FHSH. Air temperature and

precipitation data for regression model of streamflow at Huanghe'yan Hydrological Station were collected from Madoi Meteorological Station from 1976–1997.

The areal extent of permafrost in the HAYR was reviewed, integrated, and updated from the in-situ borehole data and extraction from distribution of permafrost on the QTP, which is a review and integration of existing permafrost maps compiling from multisource data, such as literature, field investigations, long-term borehole data, aerial photographs, and satellite images [24–26,47,48].

2.3. Methods

Multiple methods are capable of reconstructing streamflow [49–51], while current reconstruction methods of streamflow require much hydrometeorological data to create a statistical regressive model. For remote, high-latitudinal and high-elevational catchments with scarce data, the double mass curve method can be applied with only requirements of a set of single hydrometric data, without or with minor human disturbances [52].

The double mass curve method was developed originally for detecting the consistency of hydrometeorological data as streamflow, precipitation, and other hydroclimatic variables, and has been used to adjust or correct the inconsistent data between stations in a given area [52]. Data collected from two stations in an area with the same time series and steps were reformatted by cumulating data ahead of this dataset in a temporal sequence. The reformatted data were set as X- and Y-axis. The graph with reformatted data was presented as a straight line as long as the relation between the two variables was a fixed ratio. When the condition of one of these variable changes, such as changes in the method of data collection, or physical changes, that may affect the mutual relations between or among variables, the straight line will be curved or deflected. With similar geographical characteristics (i.e., vegetation, permafrost, and topography, among others), Zhang et al. (2004) found a close relationship for streamflow regimes between Huanghe'yan Hydrological Station and its neighboring hydrological stations in the Source Area of Yellow River (above the Tanag) [53]. Thus, the double mass curve method can be reliably applied to correct the streamflow data in the HAYR.

According to corrected data, the Yellow River flow in the HAYR is predicted for the future 20 years. Streamflow data display a complicated nonlinear pattern and are regulated by multiple factors, such as temperature, precipitation, evaporation, and basin physical conditions, among others. Streamflow predictions by employing process-based physical models need a large amount of data, strenuous model building and testing, and many proper parameters while artificial neural networks can create complex nonlinear mapping and can be adapted for detecting subtle changes in the hydroclimatic environment (Figure 4), and it has been widely used in streamflow prediction (e.g., [54–57]).
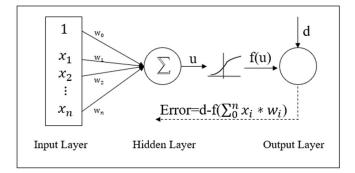

Figure 4. General layout of artificial neural network—single neuron case (adopted from [58]; input labeled with a constant 1 represents the bias term used to model the threshold; w_i: synaptic weight; input layer can be expressed as $\sum_0^n x_i * w_i$; multiple neurons and number of layers are set to nonlinearly improve the network in the hidden layer; output *f(u)* is compared with the desired target value d, and the Error is computed by the difference between *f(u)* and d; Error is minimized to derive the optimized weights w_0, w_1, $\cdots$, and w_n).

In this work, the invariant relations between hydroclimatic variables, such as precipitation, evaporation, basin physical conditions, among many others, and streamflow are presumed and changes in streamflow represents those of hydroclimatic variables. Streamflow prediction employs Elman network (Equations (1)–(3)), a recurrent artificial neural network, to predict monthly streamflow conducted in the MATLAB 2018a. Four input layer nodes, lags of flow values and 11 hidden nodes, were chosen and 70% of the series data was the default set for neural network training and 30%, for model test.

$$y(t) = f(y(t-1), y(t-2), \cdots, y(t-p)),$$ (1)

$$X = (y(t-1), y(t-2), \cdots, y(t-p)),$$ (2)

$$D = \iint \|y(t) - f(X)\|^2 P(X, y(t)) dX dy(t),$$ (3)

where, $y(t)$ is the observation of signal at time t, and $y(t-1)$, $y(t-2)$, $\cdots$, and $y(t-p)$ are previous observations of signal $y(t)$. The $f(X)$ is the neural network with a minimized prediction residual. D is the prediction residual. $P(X, y(t))$ is the density function of the joint probability of X and $y(t)$.

In this study, a trend analysis using ordinary least squares regression was also conducted to examine long-term changes in monthly, seasonal, and annual streamflow rates in the HAYR. Comparisons between pre- and post-correction streamflow trends were made to demonstrate the impacts of reservoir construction, operation, and removal on streamflow. Based on the post-correction Yellow River streamflow data in the HAYR, predicted changes in streamflow were analyzed and compared with the current flow trends to examine the future streamflow regimes.

3. Results

3.1. Reconstruction of Yellow River Streamflow Records

The subtrends of annual Yellow River streamflow in the HAYR of pre- and post-construction of the FHSH were firstly analyzed to investigate whether there is a significant difference before and after construction of the FHSH by employing the method introduced by Onyutha (2021) [59]. By reformatting the full-time series of the Yellow River streamflow datasets, a subtrend of full-time series dataset can be obtained (Figure 5e) and according to the positive or negative value of subtrend of full-time series dataset in Figure 5e, subperiods can be divided and subtrends of subperiods can be plotted as shown in Figure 5e–h. For example, in Figure 5e,i, an insignificant trend of annual streamflow in the HAYR can be found in the full-time series (1955–2019). However, since the FHSH was put into operation, a reversed trend occurred in both 1973 and 1999, i.e., before and after the construction of the FHSH. A robust two-sample t test on the pre- and post-dam streamflow (1976–1997; 1998–2006) was conducted and the p value is 0.01, which is less than 0.05. The hypothesis of equal variance of pre- and post-dam streamflow is rejected and thus there is a significant statistical difference between pre- and post-annual streamflow in the HAYR ($\alpha = 0.05$).

Thus, according to the streamflow measured at the Huanghe'yan Hydrological Station when substantially disturbed by the presence of the FHSH, especially during the periods from January 1998 to January 2007 and from October 2016 to August 2019, streamflow at the Huanghe'yan Hydrological Station was corrected by employing double mass curve method, compared with results from a regression model taking precipitation and air temperature as input variables (Figure 6). It was confirmed that the construction and operation of the FHSH has indeed disturbed the streamflow in the HAYR.
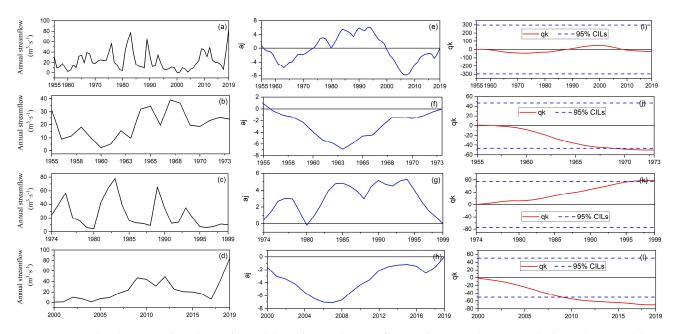
Figure 5. Graphical statistical analysis of variability of annual streamflow at the Huagnhe'yan Hydrological Station (Plots (**a**–**d**) stand for full-time series and subseries annual streamflow at Huanghe'yan; with Plots (**e**–**h**) for subtrend; charts (**i**–**l**) for significance at 95% confidence level; aj: calculated based on the concept of standard Brownian motion; qk: a step-wise summation of value a).
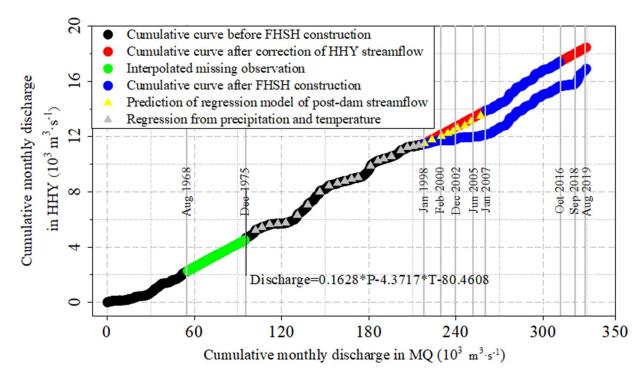

Figure 6. Double mass curve analysis between the Huanghe'yan and Maqu hydrological stations for correcting the Yellow River discharge at the Huanghe'yan near Madoi, Qinghai Province on the northeastern Qinghai-Tibet Plateau, Southwest China.

Thus, the streamflow at the Huanghe'yan Hydrological Station was corrected for the periods from January 1998 to January 2007 and from October 2016 to August 2019 in this study. A comparison of pre- and post-correction streamflow rates is shown in Figure 7. During the active dam construction period (January 1998 to February 2000), the gauged (uncorrected) streamflow in the HAYR, as measured at the Huanghe'yan

Hydrological Station, showed a reduction of 53.5–68.4% in comparison with that of the corrected streamflow (Figure 7). During the period of March 2000 to December 2002 when the FHSH was impounding water, the streamflow in the HAYR declined by 25.6–95.1% in comparison with that of the corrected streamflow. During the low-flow periods (January 2003 to June 2005), the streamflow in the HAYR showed a reduction of 71.8–94.4% in comparison with that of the corrected streamflow. From October 2016 to September 2018, the FHSH was abandoned with its water gate left partially open. The incoming water to the Yellow River was once largely preserved in the FHSH. The gauged flow rate at the Huanghe'yan Hydrological Station was reduced by 74.2% by comparing the gauged value with that of the post-correction (Figure 7). Recent dam removal of the FHSH (October 2018 to August 2019) boosted streamflow in the HAYR by 123–210% (2018–2019) in comparison with that of the post-correction. In summary, damming issues have largely altered the annual distributive patterns of streamflow in the HAYR, especially from January 1998 to January 2007 and from October 2016 to August 2019.
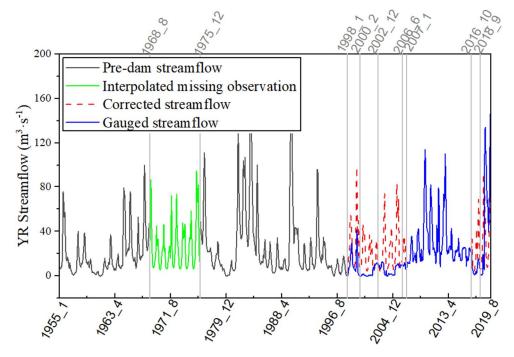

Figure 7. Comparison of measured (gauged) and corrected streamflow of the Yellow River at the Huanghe'yan Hydrological Station in the Headwater Area of the Yellow River (HAYR) on the northeastern Qinghai-Tibet Plateau, Southwest China during the period from January 1955 to August 2019.

Streamflow correction also changed the interannual trends of monthly, seasonal, and annual streamflow rates in the HAYR. Precorrection mean annual streamflow demonstrates an insignificant decreasing trend (-0.009 m^3·s^{-1}·yr^{-1}) at a 6% confidence level; it goes upwards (0.11 m^3·s^{-1}·yr^{-1}; 71% confidence level) after the streamflow correction. According to the monthly mean air temperature, precipitation, and streamflow regimes in the HAYR, hydrological season is divided to four seasons: winter (from November to next April), spring (May and June), summer (July and August), and autumn (September and October) [8]. Before correction, streamflow in spring, summer, and autumn in the HAYR show insignificant decreasing trends as -0.04 (35% confidence level), -0.18 (62% confidence level) and -0.03 m^3·s^{-1}·yr^{-1} (10% confidence level), respectively, while that in winter shows an increasing trend of 0.07 m^3·s^{-1}·yr^{-1} (60% confidence level). After correction, streamflow in the HAYR in all four seasons shows consistent and evident increasing trends: 0.16 m^3·s^{-1}·yr^{-1} in spring (94% confidence level), 0.12 m^3·s^{-1}·yr^{-1} in summer (45% confidence level), 0.16 m^3·s^{-1}·yr^{-1} in autumn (53% confidence level), and

$0.08 \text{ m}^3 \cdot \text{s}^{-1} \cdot \text{yr}^{-1}$ in winter (72% confidence level). Precorrection annual maximum and minimum streamflow rates and the ratio of the annual maximum/minimum streamflow ($Q_{\text{Max}}/Q_{\text{Min}}$) show trends of -0.11 (32% confidence level) and $-0.004 \text{ m}^3 \cdot \text{s}^{-1} \cdot \text{yr}^{-1}$ (7% confidence level) and 0.07 yr^{-1} (24% confidence level), respectively. On the contrary, post-correction annual maximum and minimum flow rates and the ratio of $Q_{\text{Max}}/Q_{\text{Min}}$ show trends of 0.18 (53% confidence level) and $0.04 \text{ m}^3 \cdot \text{s}^{-1} \cdot \text{yr}^{-1}$ (53% confidence level) and -0.08 yr^{-1} (76% confidence level), respectively.

3.2. Projection of Future Streamflow in the HAYR

By employing the method of Elman neural network, the monthly streamflow in the HAYR was forecasted over the next 20 years. Datasets during the period from December 1995–August 2019 were divided into December 1955–July 1997 and August 1997-August 2019 as train and test data. Two indicators (root mean squared error (RMSE) in $\text{m}^3 \cdot \text{s}^{-1}$ and coefficient of correlation, R, dimensionless) were employed to evaluate the performance of the trained Elman neural network [41]. The results show an RMSE of training data at $9.16 \text{ m}^3 \cdot \text{s}^{-1}$ and an R at 0.94, and an RMSE of testing data at $13.7 \text{ m}^3 \cdot \text{s}^{-1}$ and an R at 0.79. They indicate that the Elman neural network simulated monthly streamflow data fit well with the measured monthly streamflow data in the HAYR and the trained Elman neural network can effectively simulate monthly streamflow in the HAYR (Figure 8).
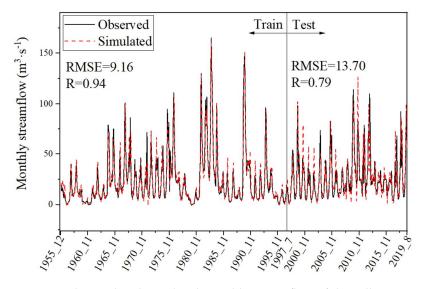

Figure 8. Observed and simulated monthly streamflow of the Yellow River at the Huanghe'yan Hydrological Station in the Headwater Area of the Yellow River on the northeastern Qinghai-Tibet Plateau, Southwest China during the period from December 1955 to August 2019.

This trained Elman neural network was then used for predicting the monthly, seasonal, and annual streamflow in the HAYR over the next 20 years, i.e., from January 2020 to December 2040 (Figure 9) and an assemble of trends and significance of uncorrected, gauged and predicted streamflow in the HAYR is shown in Table 1. Over the next 20 years, monthly, seasonal, and annual streamflow in the HAYR show consistently increasing trends, yet to varied extents.
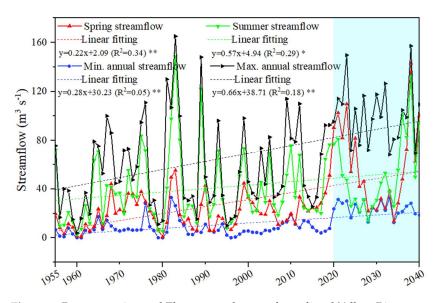
Figure 9. Post-correction and Elman neural network predicted Yellow River streamflow in the HAYR at the Huanghe'yan Hydrological Station from 1955 to 2040 (post-correction flow data from 1955 to 2019 were gauged at the Huanghe'yan Hydrological Station; data in light blue shadows are predicted annual maximum and minimum flows and summer and spring flows in the HAYR during 2020–2040 using the trained Elman neural network method; * Significant at 95% confidence level, and; ** Significant at 99% confidence level).

Table 1. Assembles of trends and significance of uncorrected, gauged and predicted streamflow at Huanghe'yan Hydrological Station in the HAYR, northeastern Qinghai-Tibet Plateau, Southwest China.

Yellow River Streamflow	Trend (in $m^3 \cdot s^{-1} \cdot yr^{-1}$) and Significance (in %)							
	Annual	**Spring**	**Summer**	**Autumn**	**Winter**	**Max.**	**Min.**	**Max./Min.**
Gauged	−0.009; 6	−0.04; 35	−0.18; 62	−0.03; 10	+0.07; 60	−0.11; 32	−0.004; 7	0.07; 24
Corrected	+0.11; 71	+0.16; 94	+0.12; 45	+0.16; 53	+0.08; 72	+0.18; 53	+0.04; 53	−0.08; 76
Predicted	+0.42; 99	+0.57; 99	+0.28; 95	+0.18; 92	+0.49; 99	+0.66; 99	0.22; 99	−0.11; 99

Note: Values in this table before and after the semicolon are trend and confidence level of trend significance, respectively.

Compared to the increasing trend (0.11 $m^3 \cdot s^{-1} \cdot yr^{-1}$) of annual streamflow in the HAYR from 1955 to 2019, a more remarkable increasing trend (0.42 $m^3 \cdot s^{-1} \cdot yr^{-1}$) is from 1955 to 2040 and annual streamflow increases by 114% from 2020 to 2040 compared to that of 1955–2019. Predicted winter flow in the HAYR shows a marked increasing trend of 0.49 $m^3 \cdot s^{-1} \cdot yr^{-1}$ from 1955 to 2040, compared to the slight increasing trends from 1955 to 2019 (0.08 $m^3 \cdot s^{-1} \cdot yr^{-1}$) and multi-year average winter streamflow from 2020 to 2040 is predicted to be 2.5 times higher than that of the period from 1955 to 2019. Predicted spring streamflow shows a more sharply increasing trend from 1955 to 2040 (0.57 $m^3 \cdot s^{-1} \cdot yr^{-1}$) in comparison with that of 1955–2019 (0.16 $m^3 \cdot s^{-1} \cdot yr^{-1}$). Spring streamflow will increase by 189% in 2020–2040 compared to that of 1955–2019. Summer and autumn streamflow will increase by 36% and 12% from 2020 to 2040 compared to those of 1955–2019, respectively and both show moderate increasing trends of 0.28 and 0.18 $m^3 \cdot s^{-1} \cdot yr^{-1}$ (1955–2040). They are higher than those from 1955 to 2019 (0.12 and 0.16 $m^3 \cdot s^{-1} \cdot yr^{-1}$, respectively). The predicted trends of 1955–2040 of annual maximum and minimum streamflow are 0.66 and 0.22 $m^3 \cdot s^{-1} \cdot yr^{-1}$, respectively, which are higher than those from 1955 to 2019 of 0.18 and 0.04 $m^3 \cdot s^{-1} \cdot yr^{-1}$, respectively. The predicted declining trend for the Q_{Max}/Q_{Min} ratio is −0.11 yr^{-1}, which is more rapid than that of −0.08 yr^{-1} from 1955 to 2019 (Table 1).

Taking into account of general increasing trends of monthly, seasonal, and annual streamflow rates, the HAYR may move into a wetting period over the next 20 years. In contrast, a more rapid decreasing trend of the Q_{Max}/Q_{Min} ratio implies that climate

warming and permafrost degradation in the HAYR may keep on substantially modifying the seasonal distributive patterns of streamflow.

3.3. Uncertainty Analysis

Streamflow prediction in this work employs the Elman neural network time-series method, which is under the assumption of invariant relations of hydroclimatic variables and physical environments. The uncertainty of prediction is estimated as ±243% according to test performance. However, climatic change and subsequent permafrost degradation alter or modify subsurface hydrogeological conditions and surface vegetation and snow covers and soil conditions, which may alter the relations of physical environment and streamflow. Degradation of permafrost and retreating of glacier may release extra ice-melt into the rivers and lakes. Thus, prediction of streamflow in the HAYR will be of large uncertainty under a warming climate in the future.

4. Discussion

The presence of the FHSH dam has changed trends of monthly, seasonal, and annual streamflow rates in the HAYR. Trends of winter baseflow increased at a rate of $0.08 \, \text{m}^3 \cdot \text{s}^{-1} \cdot \text{yr}^{-1}$ during 1955–2019, and annual minimum streamflow at a rate of $0.04 \, \text{m}^3 \cdot \text{s}^{-1} \cdot \text{yr}^{-1}$. However, the ratio of Q_{Max}/Q_{Min} decreased by $-0.08 \, \text{yr}^{-1}$ in comparison to the precorrection trends as 0.07 and $-0.004 \, \text{m}^3 \cdot \text{s}^{-1} \cdot \text{yr}^{-1}$ and $0.07 \, \text{yr}^{-1}$, respectively (Table 1).

In other basins on the QTP and in northern and boreal permafrost regions, similar streamflow regimes have been widely reported. The authors of [60] analyzed the winter baseflow and annual minimum streamflow of the upper reach of the Hei'he basin on the northeastern QTP and highlighted a notable increase of winter baseflow and annual minimum streamflow (55% and 64%·yr^{-1}, respectively). Using the hydrological model coupled with a Simultaneous Heat and Water (SHAW) model, the authors of [61] noted that the removal of permafrost module would boost winter baseflow of the upper reach of the Hei'he basin by a factor of two to three. In [62], the authors examined streamflow patterns of two subcatchments in the source area of the Yangtze River Basin and found increasing trends of winter baseflow. On the basis of Gravity Recovery and Climate Experiment (GRACE) satellite data, the authors of [63] highlighted the overall increase in water storage of catchments on the QTP (2003–2012) and the most significant increase in water storage on the QTP occurs in the zone of continuous permafrost [64]. In permafrost regions in Northeast China, decreasing trends of winter baseflow have also been frequently reported. The authors of [65] examined a boosted winter flow (1958–1998) in a subcatchment of the Heilongjiang River Basin, the northernmost boreal permafrost basin in Northeast China. In [66], significant increasing trends of winter baseflow in two permafrost catchments in the northeastern China were addressed. The authors of [16] examined the streamflow regimes in the Lena catchments in the Eastern Siberia, Russia and found downward trends of Q_{Max}/Q_{Min}. In [67], the authors investigated the minimum streamflow of 111 northern Eurasian catchments, revealing an overall pattern of increasing minimum streamflow. Lyon and Destouni (2010) investigated the changes in streamflow at subcatchments in the Yukon River Basin across Arctic Alaska and NWT, Canada, revealing a relative increase in groundwater flow [68]. More detailed information on trends of winter streamflow, Q_{Min}, and Q_{Max}/Q_{Min} in permafrost basins of northern countries and on the QTP is presented in Supplementary Material Table S1.

Permafrost soil, particularly the ice-rich permafrost one, has low hydraulic connectivity, which can greatly restrain lateral water infiltration, or to deeper soil strata [15,18,22]. Presence of permafrost will change water distribution in subsurface layers and seasonal distribution of in-stream flow [20,22,69]. With degrading permafrost, the difference between summer stormflow and winter baseflow will be reduced and the ratio of Q_{Max}/Q_{Min} will decline, flattening the annual hydrograph [8,17]. Over the next two decades (2020–2040), the trends for annual minimum streamflow ($0.22 \, \text{m}^3 \cdot \text{s}^{-1} \cdot \text{yr}^{-1}$) and for the ratio of Q_{Max}/Q_{Min} ($-0.11 \, \text{yr}^{-1}$) suggest the degrading permafrost will further impact surface and subsurface

hydrological processes. Spatiotemporal distributive patterns of water resources in the HAYR will alter due to permafrost degradation.

The corrected annual streamflow in the HAYR at Huanghe'yan demonstrates an upward trend as $0.11 \, \text{m}^3 \cdot \text{s}^{-1} \cdot \text{yr}^{-1}$, in contrast to the slight decreasing trend as $-0.009 \, \text{m}^3 \cdot \text{s}^{-1} \cdot \text{yr}^{-1}$ prior to the flow correction, and the annual streamflow in the HAYR is predicted to increase more substantially over the next 20 years ($+0.19 \, \text{m}^3 \cdot \text{s}^{-1} \cdot \text{yr}^{-1}$) (Table 1). As reported by earlier studies, in most permafrost catchments on the QTP, such as the upstreams of the Yangtze, Mekong, Yarlung Tsangpo and Salween rivers, increasing streamflow rates have been observed in recent decades [70,71]. Increase precipitation (mainly in the form of snowfall from mid-autumn to next spring) and shrinking alpine cryosphere are the major drivers for upward trends of basin streamflow on the QTP [71,72]. Modern glaciers cover an areal extent of 49,873–98,739 km^2 with an ice storage of 4561–7481 km^3 on the QTP [73,74]. The HAYR, in the absence of modern glaciers, is extensively underlain by alpine or high-plateau permafrost (86%), where ground-ice meltwater contributes to 14.4% of annual streamflow at the Huanghe'yan Hydrological Station in the HAYR [8]. Total storage of ground ice on the QTP is estimated as 9528–12,700 km^3 [75–77]. Thus, under a wetting-warming climate in the future, a trend of generally increasing annual streamflow should be expected in alpine cryosphere-dominated basins on the QTP [76]. A general increasing trend from instrumental record of streamflow to Arctic Oceans has been identified and it seems only to be more prominent in northern Eurasian and American rivers [78]. Eurasian Arctic catchments contribute 75% of the total terrestrial streamflow to the Arctic Ocean; the authors of [35] noted a 7% increase of streamflow over the period of 1939–1999, which was projected to accelerate in the 21st century. Thus, upward trends in streamflow have been observed over much of northern, alpine and high-plateau catchments.

A warm-wet climatic trend has been recorded in recent decades at the Madoi Meteorological Station in the HAYR [79]. However, the boosted precipitation occurs concentratively in winter and spring [8], which induce significantly boosted spring streamflow ($0.16 \, \text{m}^3 \cdot \text{s}^{-1} \cdot \text{yr}^{-1}$; significance at 94% confidence level) (Table 1). In most arctic and boreal basins, boosted spring streamflow has been found in the last decades [49,80]. It has been suggested that the early snow melting associated with climate warming during the snowmelt period accounts for the boosted spring streamflow rate [1,81]. In combination with the recession of permafrost, summer and autumn, streamflow also demonstrates increasing trends (0.12 and $0.16 \, \text{m}^3 \cdot \text{s}^{-1} \cdot \text{yr}^{-1}$) (Table 1). Rising trends of autumn streamflow are not so widely reported as to those of spring and winter streamflow rates, but they have also been noted in some studies [81–83] and explained as due to the shifts of nival/pluvial precipitation due to climate warming and seasonal thawing of the transient permafrost layer [83]. The declining trend of summer streamflow is often reported due to the lowered precipitation/evaporation ratio (e.g., [84]). The summer streamflow in the HAYR demonstrates a general trend of decreasing flow rate (1961–2017) in earlier studies, but it shows an increasing trend ($0.12 \, \text{m}^3 \cdot \text{s}^{-1} \cdot \text{yr}^{-1}$) when flow data are updated (1955–2019) in this paper. According to the IPCC climatic scenarios, the future warm-wet climatic trend will be continued, and trends of streamflow changes strengthened [85].

5. Conclusions

(1) Construction and operation of the FHSH have substantially resulted in the inter- and intra-annual variability of streamflow in the HAYR. Construction of the dam has caused a 53.5–68.4% reduction of annual streamflow (1998–2000) and a 71.8–94.4% reduction of annual streamflow in dry years (2003–2005) in the HAYR, and, due to the release of the previously accumulated water, the recent implementation of partial dam removal (September 2018) has boosted annual streamflow by 123–210%. Annual streamflow in the HAYR as measured at the Huanghe'yan Hydrological Station demonstrates a slight decreasing trend before correction, but a sharp upward trend after correction. Change trends of streamflow in spring, summer, autumn and winter are -0.04, -0.18, -0.03 and $+0.07 \, \text{m}^3 \cdot \text{s}^{-1} \cdot \text{yr}^{-1}$, respectively, before flow

data correction and they are +0.16, +0.12, +0.16 and +0.08 $m^3 \cdot s^{-1} \cdot yr^{-1}$, respectively, after correction.

(2) Presence of the FHSH largely has disturbed the signals of flow changes resulting from degrading permafrost in the HAYR. Permafrost alters subsurface hydrological processes and in-stream flow patterns. Winter baseflow will be boosted, but the ratio of Q_{Max}/Q_{Min} will decline in terms of thawing permafrost. Our study has yielded post-correction trends of annual minimum streamflow, winter baseflows and the ratio of Q_{Max}/Q_{Min} in the HAYR at 0.04 and 0.08 $m^3 \cdot s^{-1} \cdot yr^{-1}$ and -0.08 yr^{-1}, respectively. In comparison with the trends of precorrection annual minimum streamflow, winter baseflow and the ratio of Q_{Max}/Q_{Min} of -0.004 and 0.07 $m^3 \cdot s^{-1} \cdot yr^{-1}$ and 0.03 yr^{-1}, respectively, the post-correction streamflow has evidenced an elevated annual minimum streamflow and winter baseflow and a declined ratio of Q_{Max}/Q_{Min} (flattening hydrograph) induced by permafrost degradation. In the next 20 years, the ratio of Q_{Max}/Q_{Min} is projected to further decline at a rate of -0.11 yr^{-1}, which will be more rapid than that of -0.08 yr^{-1} from 1955 to 2019. Permafrost degradation may continue to impact subsurface hydrological processes and flows in the HAYR over the decades to come.

(3) The total streamflow in the HAYR shows a generally increasing trend (0.11 $m^3 \cdot s^{-1} \cdot yr^{-1}$) over the past decades (1955–2019) and may have a more prominent increasing trend (0.42 $m^3 \cdot s^{-1} \cdot yr^{-1}$) in the future (1955–2040). Together with a changing climate, a warmer-wetter HAYR should be expected, as observed in other QTP catchments. Increasing precipitation and shrinking alpine cryosphere are concerned as the major drivers for upward trends of basin streamflow on the QTP. Boosted change trends of spring flow (0.57 $m^3 \cdot s^{-1} \cdot yr^{-1}$) and autumn flow (0.22 $m^3 \cdot s^{-1} \cdot yr^{-1}$) may reveal the advancing snow-melt season and postponing freeze-up, and subsequently a potential expansion of growing season. They will naturally benefit ecological restoration and ecological environment. These hydrometeorological and ecological trends in the HAYR may also help enhance ecological safety and water supply in local communities and the downstream Yellow River basins.

References

1. Ye, B.; Yang, D.; Kane, D.L. Changes in Lena River streamflow hydrology: Human impacts versus natural variations. *Water Resour. Res.* **2003**, *39*, 1200. [CrossRef]
2. Adam, J.C.; Haddeland, I.; Su, F.; Lettenmaier, D.P. Simulation of reservoir influences on annual and seasonal streamflow changes for the Lena, Yenisei, and Ob' rivers. *J. Geophys. Res.* **2007**, *112*, D24114. [CrossRef]
3. Stuefer, S.; Yang, D.; Shiklomanov, A. Effect of streamflow regulation on mean annual discharge variability of the Yenisei River. In *Cold Regions Hydrology in a Changing Climate*; Yang, D., Marsh, P., Gelfan, A., Eds.; IAHS: Melbourne, Australia, 2011.
4. Chai, Y.; Li, Y.; Yang, Y.; Zhu, B.; Li, S.; Xu, C.; Liu, C. Influence of climate variability and reservoir operation on streamflow in the Yangtze River. *Sci. Rep.* **2019**, *9*, 5060. [CrossRef] [PubMed]
5. Jin, H.; He, R.; Cheng, G.; Wu, Q.; Wang, S.; Lü, L.; Chang, X. Changes in frozen ground in the Source Area of the Yellow River on the Qinghai–Tibet Plateau, China, and their eco-environmental impacts. *Environ. Res. Lett.* **2009**, *4*, 045206. [CrossRef]
6. Ge, S.; Yang, D.; Kane, D.L. Yukon River Basin long-term (1977–2006) hydrologic and climatic analysis. *Hydrol. Process.* **2013**, *27*, 2475–2484. [CrossRef]
7. Bring, A.; Shiklomanov, A.; Lammers, R.B. Pan-Arctic river discharge: Prioritizing monitoring of future climate change hot spots. *Earth Future* **2017**, *5*, 72–92. [CrossRef]
8. Ma, Q.; Jin, H.; Bense, F.V.; Luo, D.; Marchenko, S.; Harris, A.; Lan, Y. Impacts of degrading permafrost on streamflow in the source area of Yellow River on the Qinghai-Tibet Plateau, China. *Adv. Clim. Chang. Res.* **2019**, *10*, 225–239. [CrossRef]
9. Jin, H.J.; Jin, X.Y.; He, R.X.; Luo, D.L.; Chang, X.L.; Wang, S.L.; Harris, S.A. Evolution of permafrost in China during the last 20 ka. *Sci. China Earth Sci.* **2019**, *62*, 1207–1223. [CrossRef]
10. Cheng, G.; Jin, H. Permafrost and groundwater on the Qinghai-Tibet Plateau and in northeast China. *Hydrogeol. J.* **2012**, *21*, 5–23. [CrossRef]
11. Bring, A.; Destouni, G. Arctic climate and water change: Model and observation relevance for assessment and adaptation. *Surv. Geophys.* **2014**, *35*, 853–877. [CrossRef]
12. Haine, T.W.N.; Curry, B.; Gerdes, R.; Hansen, E.; Karcher, M.; Lee, C.; Spreen, G.; de Steur, L.; Stewart, K.; Woodgate, R. Arctic freshwater export: Status, mechanisms, and prospects. *Glob. Planet. Chang.* **2015**, *125*, 13–35. [CrossRef]
13. Kurylyk, B.L.; Hayashi, M.; Quinton, W.L.; McKenzie, J.M.; Voss, C.I. Influence of vertical and lateral heat transfer on permafrost thaw, peatland landscape transition, and groundwater flow. *Water Resour. Res.* **2016**, *52*, 1286–1305. [CrossRef]
14. Prowse, T.D.; Wrona, F.J.; Reist, J.D.; Gibson, J.J.; Hobbie, J.E.; Le'vesque, L.M.J.; Vincent, W.F. Climate change effects on hydroecology of Arctic freshwater ecosystems. *Ambio* **2006**, *35*, 347–358. [CrossRef]
15. Ye, B.; Yang, D.; Zhang, Z.; Kane, D.L. Variation of hydrological regime with permafrost coverage over Lena Basin in Siberia. *J. Geophy. Res.* **2009**, *114*, D07102. [CrossRef]
16. Ye, B.; Yang, D.; Zhang, T.; Zhang, Y.; Zhou, Z. 2011 Hydrological process change with air temperature over the Lena Basin in Siberia. In Proceedings of the Cold Regions Hydrology in a Changing Climate, Melbourne, Australia, 25 July 2011.
17. Ye, B.; Ding, Y.; Jiao, K.; Shen, Y.; Zhang, J. The response of river discharge to climate warming in cold region over China. *Quatern. Sci.* **2012**, *32*, 103–110. (In Chinese)
18. Bense, V.F.; Kooi, H.; Ferguson, G.; Read, T. Permafrost degradation as a control on hydrogeological regime shifts in a warming climate. *J. Geophy. Res. Earth* **2012**, *117*, F03036. [CrossRef]
19. Thawing Permafrost Reduces River Runoff? Available online: https://www.nature.com/news/thawing-permafrost-reduces-river-runoff-1.9749 (accessed on 6 January 2020).
20. Kane, D.L.; Yoshikawa, K.; McNamara, J.P. Regional groundwater flow in an area mapped as continuous permafrost, NE Alaska (USA). *Hydrogeol. J.* **2013**, *21*, 41–52. [CrossRef]
21. Han, T.; Pu, H.; Cheng, P.; Jiao, K. Hydrological effects of alpine permafrost in the headwaters of the Urumqi River, Tianshan Mountains. *Sci. Cold Arid Reg.* **2016**, *8*, 241–249.
22. Walvoord, M.A.; Kurylyk, B.L. Hydrologic impacts of thawing permafrost—A review. *Vadose Zone J.* **2016**, *15*, 1–20. [CrossRef]
23. Xu, R.; Hu, H.; Tian, F.; Li, C.; Khan, M.Y.A. Projected climate change impacts on future streamflow of the Yarlung Tsangpo-Brahmaputra River. *Glob. Planet. Chang.* **2019**, *175*, 144–159. [CrossRef]
24. Li, J.; Sheng, Y.; Wu, J.; Feng, Z.; Hu, X.; Zhang, X. Landform-related permafrost characteristics in the source area of the Yellow River, eastern Qinghai-Tibet Plateau. *Geomorphology* **2016**, *269*, 104–111. [CrossRef]
25. Wang, S.; Sheng, Y.; Li, J.; Wu, J.; Cao, W.; Ma, S. An estimation of ground ice volumes in permafrost layers in Northeastern Qinghai-Tibet Plateau, China. *Chin. Geogr. Sci.* **2018**, *28*, 61–73. [CrossRef]
26. Sheng, Y.; Ma, S.; Cao, W.; Wu, J. Spatiotemporal changes of permafrost in the Headwater Area of the Yellow River under a changing climate. *Land Degrad. Dev.* **2020**, *31*, 133–152. [CrossRef]
27. Liu, J.; Duan, Y.; Hao, G.; Ge, X.; Sun, H. Evolutionary history and underlying adaptation of alpine plants on the Qinghai-Tibet Plateau. *J. Syst. Evol.* **2014**, *52*, 241–249. [CrossRef]
28. Jin, X.; Jin, H.; Wu, X.; Luo, D.; Sheng, Y.; Li, X.; He, R.; Wang, Q.; Knops, J.M.H. Permafrost degradation leads to decrease in biomass and species richness on the northeastern Qinghai-Tibet Plateau. *Plants* **2020**, *9*, 1453. [CrossRef]
29. Li, Z.; Liu, X.; Niu, T.; De, K. Ecological restoration and its effects on a regional climate: The Source Region of the Yellow River, China. *Environ. Sci. Technol.* **2015**, *49*, 5897–5904. [CrossRef]

30.　Jin, X.; Jin, H.; Iwahana, G.; Marchenko, S.; Luo, D.; Li, X.; Liang, S. Impacts of climate-induced permafrost degradation on vegetation: A review. *Adv. Clim. Chang. Res.* **2020**, *12*, 29–47. [CrossRef]

31.　Gao, S.; Jin, H.; Bense, V.F.; Wang, X.; Chai, X. Application of electrical resistivity tomography for delineating permafrost hydrogeology in the headwater area of Yellow River on Qinghai-Tibet Plateau, SW China. *Hydrogeol. J.* **2019**, *27*, 1725–1737. [CrossRef]

32.　Serban, D.R.; Jin, H.; Serban, M.; Luo, D.; Wang, Q.; Jin, X.; Ma, Q. Mapping thermokarst lakes/ponds across permafrost landscapes in the Headwater Area of Yellow River on NE Qinghai-Tibet Plateau. *Int. J. Remote Sens.* **2020**, *41*, 7042–7067. [CrossRef]

33.　Campbell, T.K.F.; Lantz, T.C.; Fraser, R.H.; Hogan, D. High Arctic vegetation change mediated by hydrological conditions. *Ecosystems* **2020**, *23*, 106–121. [CrossRef]

34.　Xu, W.; Yang, D.; Li, Y.; Xiao, R. Correlation analysis of Mackenzie River discharge and NDVI relationship. *Can. J. Remote Sens.* **2016**, *42*, 292–306. [CrossRef]

35.　Shiklomanov, A.I.; Lammers, R.B.; Lettenmaier, D.P.; Polischuk, Y.M.; Savichev, O.G.; Smith, L.C.; Chernokulsky, A.V. Hydrological changes: Historical analysis, contemporary status, and future projections. In *Regional Environmental Changes in Siberia and Their Global Consequences*; Groisman, P.Y., Gutman, G., Eds.; Springer: Dordrecht, The Netherlands, 2013; pp. 111–154.

36.　Zeng, F.; Collatz, G.J.; Pinzon, J.E.; Ivanoff, A. Evaluating and quantifying the climate-driven interannual variability in Global Inventory Modeling and Mapping Studies (GIMMS) Normalized Difference Vegetation Index (NDVI3g) at global scales. *Remote Sens.* **2013**, *5*, 3918–3950. [CrossRef]

37.　Wang, W.; Dong, Z.; Lall, U.; Dong, N.; Yang, M. Monthly streamflow simulation for the headwater catchment of the Yellow River Basin with a hybrid statistical-dynamic model. *Water Resour. Res.* **2019**, *55*, 7606–7621. [CrossRef]

38.　Ministry of Water Resources of the People's Republic of China. *Bulletin of River Sediment in China*; China Water&Power Press: Beijing, China, 2008–2017. (In Chinese)

39.　Luo, D.; Jin, H.; Lin, L.; He, R.; Yang, S.; Chang, X. Progress in permafrost temperature and thickness in the source area of the Huanghe River. *Sci. Geogr. Sin.* **2012**, *32*, 898–904. (In Chinese)

40.　Luo, D.; Jin, H.; Marchenko, S.; Romanovsky, V. Distribution and changes of active layer thickness (ALT) and soil temperature (TTOP) in the source area of the Yellow River using the GIPL model. *Sci. China Earth Sci.* **2014**, *57*, 1834–1845. [CrossRef]

41.　Jin, H.; Luo, D.; Wang, S.; Lü, L.; Wu, J. Spatiotemporal variability of permafrost degradation on the Qinghai-Tibet Plateau. *Sci. Cold Arid Reg.* **2011**, *3*, 0281–0305.

42.　Luo, D.; Jin, H.; Jin, X.; He, R.X.; Li, X.; Muskett, R.; Marchenko, S.; Romanovsky, V. Elevation-dependent thermal regime and dynamics of frozen ground in the Bayan Har Mountains, northeastern Qinghai-Tibet Plateau, southwest China. *Permafr. Periglac. Process.* **2018**, *29*, 257–270. [CrossRef]

43.　Wang, G.; Wang, Y.; Li, Y.; Cheng, H. Influences of alpine ecosystem responses to climatic change on soil properties on the Qinghai–Tibet Plateau, China. *Catena* **2007**, *70*, 506–514. [CrossRef]

44.　Liang, S.; Ge, S.; Wan, L.; Xu, D. Characteristics and causes of vegetation variation in the source regions of the Yellow River, China. *Int. J. Remote Sens.* **2012**, *33*, 1529–1542. [CrossRef]

45.　Brierley, G.J.; Li, X.L.; Cullum, C.; Gao, J. Landscape and ecosystem diversity in the Yellow River Source Zone. In *Landscape and Ecosystem Diversity, Dynamics and Management in the Yellow River Source Zone*; Brierley, G.J., Li, X., Cullum, C., Gao, J., Eds.; Springer Geography: Cham, Switzerland, 2016; pp. 1–34.

46.　Du, Y. *Land Cover of Tibet Plateau*; National Tibetan Plateau Data Center: Beijing, China, 2019.

47.　Zheng, G.; Yang, Y.; Yang, D.; Dafflon, B.; Lei, H.; Yang, H. Satellite-based simulation of soil freezing/thawing processes in the northeast Tibetan Plateau. *Remote Sens. Environ.* **2019**, *231*, 11269. [CrossRef]

48.　Luo, D.; Liu, L.; Jin, H.J.; Wang, X.; Chen, F. Characteristics of ground surface temperature at Chalaping in the Source Area of the Yellow River, northeast Tibetan Plateau. *Agr. For. Meteorol.* **2020**, *281*, 10819. [CrossRef]

49.　Yang, D.; Ye, B.; Kane, D.L. Streamflow changes over Siberian Yenisei River Basin. *J. Hydrol.* **2004**, *296*, 59–80. [CrossRef]

50.　Hernández-Henríquez, M.A.; Mlynowski, T.J.; Déry, S.J. Reconstructing the natural streamflow of a regulated river: A case study of La Grande Rivière, Québec, Canada. *Can. Water Resour. J.* **2010**, *35*, 301–316. [CrossRef]

51.　Zhao, G.; Li, E.; Mu, X.; Wen, Z.; Rayburg, S.; Tian, P. Changing trends and regime shift of streamflow in the Yellow River basin. *Stoch. Environ. Res. Risk Assess.* **2015**, *29*, 1331–1343. [CrossRef]

52.　Searcy, J.K.; Hardison, C.H. Double-mass curves. In *Manual of Hydrology: Part I: General Surface-Water Techniques*; U.S. Geological Survey, Ed.; U. S. Government Printing Office: Washington, DC, USA, 1960; pp. 13–59.

53.　Zhang, S.; Jia, S.; Liu, C.; Cao, W.; Hao, F.; Liu, J.; Yan, H. Study on the changes of water cycle and its impacts in the source region of the Yellow River. *Sci. China Ser. E Technol. Sci.* **2004**, *47*, 142–151. [CrossRef]

54.　Birkundavyi, S.; Labib, R.; Trung, H.T.; Rousselle, J. Performance of neural networks in daily streamflow forecasting. *J. Hydrol. Eng.* **2002**, *7*, 392. [CrossRef]

55.　Dolling, O.R.; Varas, E.A. Artificial neural networks for streamflow prediction. *J. Hydraul. Res.* **2002**, *40*, 547–554. [CrossRef]

56.　Sahoo, A.; Samantaray, S.; Ghose, D.K. Stream flow forecasting in Mahanadi River Basin using artificial neural networks. *Comput. Sci.* **2019**, *157*, 168–174. [CrossRef]

57.　Sequoira, H.; Luna, I. Performance comparison of feedforward neural networks applied to streamflow series forecasting. *Mathemat. Eng. Sci. Aerosp.* **2019**, *10*, 41–53.

58. Liao, Y.; Moody, J.; Wu, L. Application of artificial neural networks to time series prediction. In *Handbook of Neural Network Signal Processing*; Hu, Y., Hwang, J., Eds.; CRC Press: Boca Raton, FL, USA, 2002; pp. 249–266.

59. Onyutha, C. Graphical-statistical method to explore variability of hydrological time series. *Hydrol. Res.* **2021**, *52*, 266–283. [CrossRef]

60. Wang, X.; Chen, R.; Liu, G.; Han, C.; Yang, Y.; Song, Y.; Guo, S. Response of low flows under climate warming in high-altitude permafrost regions in western China. *Hydrol. Process.* **2019**, *33*, 66–75. [CrossRef]

61. Zhang, Y.; Cheng, G.; Li, X.; Jin, H.; Yang, D.; Flerchinger, G.N.; Change, X.; Bense, V.; Han, X.; Liang, J. Influences of frozen ground and climate change on hydrological processes in an alpine watershed: A case study in the upstream area of the Hei'he River, Northwest China. *Permafr. Periglac. Process.* **2017**, *28*, 420–432. [CrossRef]

62. Song, C.; Wang, G.; Mao, T.; Dai, J.; Yang, D. Linkage between permafrost distribution and river runoff changes across the Arctic and the Tibetan Plateau. *Sci. China Earth Sci.* **2019**, *62*, 1–11. [CrossRef]

63. Guo, J.; Mu, D.; Liu, X.; Yan, H.; Sun, Z.; Guo, B. Water storage changes over the Tibetan Plateau revealed by GRACE mission. *Acta Geophys.* **2016**, *64*, 463–476. [CrossRef]

64. Xu, M.; Kang, S.; Zhao, Q.; Li, J. Terrestrial water storage changes of permafrost in the Three-River Source Region of the Tibetan Plateau, China. *Adv. Meteorol.* **2016**, *1*, 1–13. [CrossRef]

65. Liu, J.; Hayakawa, N.; Lu, M.; Dong, S.; Yuan, J. Winter streamflow, ground temperature and active-layer thickness in Northeast China. *Permafr. Periglac. Process.* **2003**, *14*, 11–18. [CrossRef]

66. Duan, L.; Man, X.; Kurylyk, B.L.; Cai, T. Increasing winter baseflow in response to permafrost thaw and precipitation regime shifts in northeastern China. *Water* **2017**, *9*, 1–15. [CrossRef]

67. Smith, L.; Pavelsky, T.; MacDonald, G.; Shiklomanov, A.; Lammers, R. Rising minimum daily flows in northern Eurasian rivers: A growing influence of groundwater in the high-latitude hydrologic cycle. *J. Geophys. Res. Biogeosci.* **2007**, *112*, G04S47. [CrossRef]

68. Lyon, S.W.; Destouni, G. Changes in catchment-scale recession flow properties in response to permafrost thawing in the Yukon River Basin. *Int. J. Climatol.* **2010**, *30*, 2138–2145. [CrossRef]

69. Woo, M.K. *Permafrost Hydrology*; Springer Science & Business Media: Heidelberg, Germany, 2012.

70. Lan, C.; Zhang, Y.X.; Zhu, F.X.; Liang, L.Q. Characteristics and changes of streamflow on the Tibetan Plateau: A review. *J. Hydrol. Reg. Stud.* **2014**, *2*, 49–68.

71. Liu, W.; Sun, F.; Li, Y.; Zhang, G.; Sang, Y.; Lim, W.H.; Liu, J.; Wang, H.; Bai, P. Investigating water budget dynamics in 18 river basins across the Tibetan Plateau through multiple datasets. *Hydrol. Earth Syst. Sci.* **2018**, *22*, 351–371. [CrossRef]

72. Tang, Q.; Lan, C.; Su, F.; Liu, X.; Sun, H.; Ding, J.; Wang, L.; Leng, G.; Zhang, Y.; Sang, Y.; et al. Streamflow change on the Qinghai-Tibet Plateau and its impacts. *Chin. Sci. Bull.* **2019**, *64*, 2807–2821. (In Chinese)

73. Yao, T.D.; Qin, D.H.; Shen, Y.; Zhao, L.; Wang, N.L.; Lu, X. Cryospheric changes and their impacts on regional water cycle and ecological conditions in the Qinghai-Tibetan Plateau. *Chin. J. Nat.* **2013**, *35*, 179–186. (In Chinese)

74. Wang, N.; Yao, T.; Xu, Q.; Chen, A.; Wang, W. Spatial patterns, trend and influence of glacier change in Tibetan Plateau and surroundings after global warming. *Bull. Chin. Acad. Sci.* **2019**, *34*, 1220–1232. (In Chinese)

75. Zhao, L.; Ding, Y.; Liu, G.; Wang, S.; Jin, H. Estimates of the reserves of ground ice in permafrost regions on the Tibetan Plateau. *J. Glaciol. Geocryol.* **2010**, *22*, 106–112. (In Chinese)

76. Zhao, L.; Hu, G.; Zou, D.; Wu, X.; Ma, L.; Sun, Z.; Yuan, L.; Zhou, H.; Liu, S. Permafrost changes and their effects on hydrological processes on the Qinghai-Tibet Plateau. *Bull. Chin. Acad. Sci.* **2019**, *34*, 1223–1246.

77. Cheng, G.; Zhao, L.; Li, R.; Wu, X.; Sheng, Y.; Hu, G.; Zou, D.; Jin, H.; Li, X.; Wu, Q. Characteristics, changes and impacts of permafrost on the Qinghai-Tibet Plateau. *Chin. Sci. Bull.* **2019**, *64*, 2783–2795.

78. Durocher, M.; Requena, A.I.; Burn, D.; Pellerin, J. Analysis of trends in annual streamflow to the Arctic Ocean. *Hydrol. Process.* **2019**, *33*, 1143–1151. [CrossRef]

79. Luo, D.; Jin, H. Variations of air temperature and precipitation from 1953 to 2012 in the Madoi Station in the Source Area of the Yellow River. *J. Arid Land Res. Environ.* **2014**, *28*, 1–8. (In Chinese)

80. Ahmed, R.; Prowse, T.; Dibike, Y.; Bonsal, B.; O'Neil, H. Recent trends in freshwater influx to the Arctic Ocean from four major Arctic-draining rivers. *Water* **2020**, *12*, 1–13. [CrossRef]

81. Makarieva, O.; Nesterova, N.; Post, D.A.; Sherstyukov, A.; Lebedeva, L. Warming temperatures are impacting the hydrometeorological regime of Russian rivers in the zone of continuous permafrost. *The Cryosphere* **2019**, *13*, 1635–1659. [CrossRef]

82. Caine, N. Recent hydrologic change in a Colorado alpine basin: An indicator of permafrost thaw? *Ann. Glaciol.* **2010**, *51*, 130–134. [CrossRef]

83. Kopysov, S.; Erofeev, A. The influences of climate on runoff: A case study of four catchments in Western Siberia. *Earth Environ. Sci.* **2019**, *381*, 012046. [CrossRef]

84. Spence, C.; Kokelj, S.V.; Ehsanzadeh, E. Precipitation trends contribute to streamflow regime shifts in northern Canada. In *Cold Regions Hydrology in a Changing Climate*; Yang, D., Marsh, P., Gelfan, A., Eds.; IAHS: Melbourne, Australia, 2011.

85. Chen, D.; Xu, Q.; Yao, T.; Guo, Z.; Cui, P.; Chen, F.; Zhang, R.; Zhang, X.; Zhang, Y.; Fan, J.; et al. Assessment of past, present and future environmental changes on the Tibetan Plateau. *Chin. Sci. Bull.* **2015**, *60*, 3025–3035. (In Chinese)